

1 High spatiotemporal resolution traffic CO₂ emission maps derived 2 from Floating Car Data (FCD) for 20 European cities (2023)

3
4 Qinren Shi¹, Philippe Ciais¹, Nicolas Megel², Xavier Bonnemaizon¹, Rohith Teja Mittakola¹, Richard
5 Engelen³, Chuanlong Zhou¹
6 ¹Le Laboratoire des Sciences du Climat et de l'Environnement, Saint-Aubin, 91190, France
7 ²NEXQT SAS, Paris, France
8 ³ECMWF, Robert-Schuman-Platz 3, 53175 Bonn, Germany
9

10 *Correspondence to:* Qinren Shi(qinrenshi2025@gmail.com) & Chuanlong Zhou(chuanlong.zhou@lsce.ipsl.fr)

11 **Abstract.** On-road transportation is a major contributor to CO₂ emissions in cities, and high-resolution CO₂ traffic emission
12 maps are essential for analyzing emission patterns and characteristics. In this study, we developed new hourly on-road CO₂
13 emission maps with aat 100 × 100 m resolution for 20 major cities in France, Germany, and the Netherlands in 2023. We used
14 commercial Floating Car Data (FCD) based on anonymized GPS signals periodically reported by individual vehicles,
15 providing hourly information on mean speed and on the number of GPS sample counts per street. Machine learning models
16 were developed to fill FCD data gaps and convert sample counts into actual traffic volumes, and the COPERT model was used
17 to estimate speed- and vehicle-type-dependent emission factors. These models were calibrated using independent traffic
18 observations available for Paris and Berlin, and subsequently applied to the remaining 18 cities in an extrapolated manner due
19 to data availability constraints. Hourly emissions, initially estimated at the street level, were aggregated to 100 × 100 m grid
20 cells. Annual on-road CO₂ emissions across the 20 European cities in 2023 ranged from 0.4 to 7.9 Mt CO₂, with emissions
21 strongly correlated with urban area ($R^2 = 0.98$) and, to a lesser extent, population size ($R^2 = 0.74$). Spatially, emissions are
22 either highly concentrated along major highways in cities such as Paris and Amsterdam or more evenly distributed in cities
23 such as Berlin and Bordeaux, highlighting the need for context-specific mitigation strategies. Temporally, this study shows the
24 CO₂ emission fluctuations due to holiday periods, weekly activity cycles, and distinct usage profiles of different vehicle types.
25 Due to the low latency of FCD, this approach could support near-real-time traffic emission mapping in the future. Our approach
26 enhances the spatial and temporal characterization of CO₂ emissions in on-road transportation compared to the conventional
27 method used in gridded inventories, indicating the potential of FCD data for near-real-time urban emission monitoring and
28 timely policy-making. The datasets generated by this study are available on Zenodo
29 <https://doi.org/10.5281/zenodo.16600210>(Shi et al., 2025).

3 Formatted: English (United Kingdom)

30 Formatted: Font: (Asian) +Body Asian (宋体), (Asian) Chinese
(Simplified, Mainland China), Not Highlight

31
32

33 **1 Introduction**

34 The road transport sector is one of the largest sources of greenhouse gas (GHG) emissions in the European Union and the only
35 major economic sector where carbon dioxide (CO₂) emissions have risen since 1990, primarily due to the widespread use of
36 fossil fuel-powered passenger cars and freight vehicles. In 2023, it accounts for approximately 26.0% of total EU GHG
37 emissions (EEA, 2024a). In response to the dual challenge of reducing emissions and developing cleaner mobility
38 infrastructures, the European Strategy for Low-Emission Mobility outlines three elements: (1) Increasing the efficiency of the
39 transport system, including the optimization of logistics and intelligent transport systems; (2) Accelerating the deployment of
40 low-emission alternative energy sources, such as biofuels, renewable electricity, and hydrogen; and (3) Speeding up the
41 transition to zero-emission vehicles, through regulatory incentives, infrastructure investment, and innovation support
42 (European Commission, 2016). This transition is not only critical for achieving the EU's climate neutrality goal, which
43 involves reducing net CO₂ emissions to zero by 2050 (EEA, 2024b), but also for improving air quality, reducing energy
44 dependence on fossil fuel imports, and enhancing the competitiveness of European industry.

45

46 Emission reduction targets in the transportation sector are being translated into concrete actions at the city level. For instance,
47 the transportation sector is responsible for approximately 20% of Paris' local greenhouse gas emissions (Albarus et al., 2025),
48 and Paris plans to reduce its direct emissions by 50% by 2030 and 100% by 2050, compared to 2004. The transport sector,
49 responsible for approximately 20% of Paris' local greenhouse gas emissions (Albarus et al., 2025). Paris has set itself the target
50 of phasing out diesel-powered mobility by 2024 and petrol-powered mobility by 2030, aligning with the EU-wide ban on the
51 sale of internal combustion engine vehicles by 2035. In addition, the city is developing financial incentives and support
52 measures for low-carbon mobility. It is also preparing a low-carbon urban logistics plan for the Paris region between now and
53 2030 (UNFCCC, 2023). Amsterdam aims to achieve zero-emission transport by 2030, phasing out all fossil-fuel vehicles within
54 city limits (Amsterdam, 2024). The city is rapidly expanding its electric vehicle infrastructure, as all newly registered vehicles
55 are required to have zero-emission engines in 2025 (CINEA, 2025). Over 70% of trips are already made by walking, cycling,
56 or public transport, making Amsterdam a leader in sustainable urban mobility. Similarly, to achieve climate neutrality in 2050,
57 Berlin will require a long-term reduction in CO₂ emissions in the transport sector to around 1.17 million tonnes of CO₂ per
58 year, a reduction of around 77 % compared with 1990 emissions (diBEK, 2025).

59

60 High-resolution emission maps are crucial for monitoring emission changes and providing insights into the effectiveness of
61 traffic mitigation policies in cities. For example, a high-resolution (1 km²) CO₂ emissions inventory for U.S. road transportation
62 named DARTE enables detailed analysis at the city scale between 1980 to 2012 (Gately et al., 2015), revealing that urban

Formatted: Font: (Asian) +Body Asian (宋体), (Asian) Chinese (Simplified, Mainland China)

Formatted: Font: (Default) Times New Roman, (Asian) Times New Roman

63 areas drive most of the emission growth and that traditional population-based downscaling methods substantially misrepresent
64 city-level spatial patterns. Over the past decade, several efforts have been made to improve either the temporal or the spatial
65 resolution of traffic emission inventories, primarily by incorporating real-world traffic data generated from sensors or GPS
66 signals. From a temporal resolution perspective, annual aggregated statistics make it impossible to capture short-term
67 variations due to weather, policy changes, or special events. Therefore, daily or hourly data were increasingly applied to
68 improve the accuracy. For example, TomTom collects all the travel times and compares them with the lowest travel times to
69 calculate congestion indexes based on FCD.(index, 2024). Tomtom congestion indexes were used by Carbon Monitor Cities
70 (Huo et al., 2022) to estimate daily CO₂ emissions for 1500 cities. CAMS-TEMPO is a dataset of European emission temporal
71 profiles that provides gridded monthly, daily, weekly, and hourly weight factors for atmospheric chemistry modelling, and the
72 European part used hourly traffic data collected from over 20 European cities via open-data portals or personal communications
73 (Guevara et al., 2021). One-month GPS-based datasets covering 52,834 conventional fuel vehicles registered in the province
74 of Modena and 40,459 vehicles registered in the province of Firenze were used to generate high-resolution emission maps.(De
75 Gennaro et al., 2016). A near-real-time on-road traffic emission product on 2860 km of the main roads in Bangkok was
76 automatically generated by retrieving the traffic data from the Google Maps API service and the Python code every 15 min
77 (Naiudomthum et al., 2022). In recent years, machine learning-based bottom-up approaches have supported the development
78 of high-resolution emission maps. For instance, an hourly street-level emission map of Chengdu was developed using data
79 from 1,454 camera-based sensors and 34 highway monitoring sites, employing land-use random forest models.(Wen et al.,
80 2022). Similarly, a platform tracking hourly CO₂ emissions at a 30×30 m resolution was designed for Berlin based on local
81 traffic data, using machine learning methods.(Anjos and Meier, 2025).

82

83 Despite recent advancements, most city-level emission datasets still suffer from limitations in either temporal or spatial
84 resolution, with few achieving both simultaneously. CAMS-TEMPO.(Guevara et al., 2021) and Carbon Monitor.(Huo et al.,
85 2022) lack road-specific information and provide only outputs at 0.1° resolution and the city level, respectively. The hourly
86 street-level emission datasets for Chengdu.(Wen et al., 2022) and Bangkok.(Naiudomthum et al., 2022) only cover one to two
87 months. The Berlin platform offers high spatial and temporal resolution from 2015 to 2022, but may miss data from smaller
88 roads, as counting stations are usually located on major roads.

89

90 As part of the Copernicus Atmosphere Monitoring Service (CAMS), this study estimates for the first time hourly street-level
91 on-road transportation CO₂ emissions, aggregated into 100 m resolution hourly maps for 20 European cities in 2023. Hourly
92 GPS-based data, reporting traffic counts and speeds of individual vehicles across different road classes, were upscaled using
93 machine learning to reconstruct complete traffic volumes and speeds across the road networks. Then, CO₂ emissions were
94 estimated using the COPERT model, and emission maps were developed. This approach enhances the spatial and temporal
95 characterization of CO₂ emissions in on-road transportation compared to the downscaling method used in other inventories,

96 indicating the potential of GPS-based data for supporting future efforts in emission monitoring and developing emission
97 reduction policies.

98 **2 Data and Method**

99 **2.1 Overview of the Methodology**

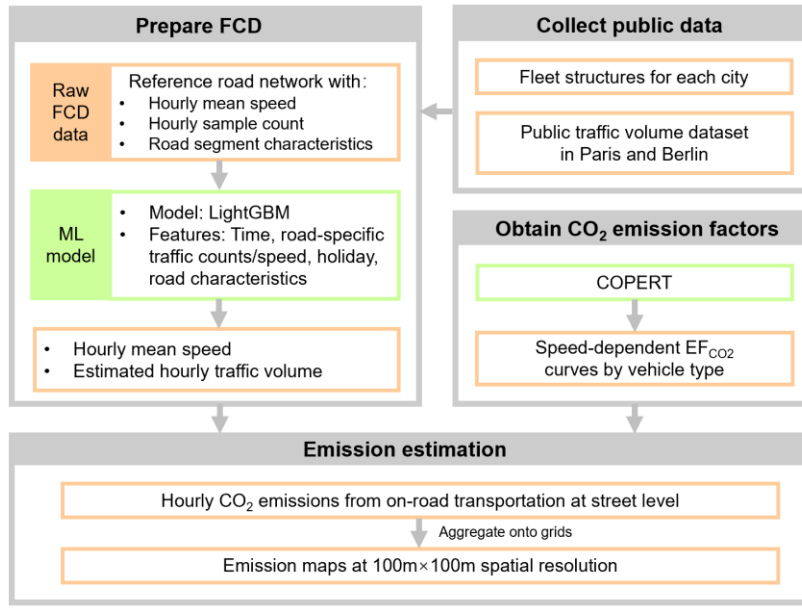
100 Figure 1 describes the [workflow methodology](#) of this study. The GPS-based high-resolution ‘Floating Car Data’ (FCD) on
101 individual vehicle flow (GPS vehicles counts per street each hour) and speed covering every street was obtained from a data
102 aggregation provider that collects GPS position data from cars (passenger cars) and trucks (light commercial vehicles and
103 heavy duty trucks), providing road-specific information on hourly average speed and sample counts (i.e., the number of cars
104 recorded in each street for each hour). Those GPS data are linked with precise cities’ road network datasets, providing detailed
105 information on road length, road functional class, and truck access authorization. All data is anonymized by the data provider
106 to prevent compromising any individual or organizational data privacy issues. After raw data processing and cleaning, a
107 machine learning model was used to fill in missing values in FCD, as well as to transform FCD sample counts limited to
108 vehicles equipped with GPS into traffic volumes for all vehicles. Then, the COPERT model (Ntziachristos et al., 2009), the
109 EU standard vehicle emissions calculator, was applied for estimating specific CO₂ emission factors based on individual vehicle
110 hourly average speed and type. Combined with the road lengths obtained from geographical databases and with fleet structures,
111 we finally estimate street-level road-specific emissions using the following equation:

$$Emis_{t,v,r} = N_{t,r} \times Structure_v \times Length_r \times EF_{v,s} \quad (1)$$

112 Where $Emis_{t,v,r}$ represents CO₂ emission at the hour t , for the vehicle type v , on road r . $N_{t,r}$ represents the total traffic
113 volume at hour t , on road r (counts/hour). $Structure_v$ represents the proportion of vehicle type v in the vehicle fleet (%).
114 $Length_r$ represents the road length (km) of the road r , and $EF_{v,s}$ (g CO₂/km) represents the CO₂ emission factors for the vehicle
115 type v , at the hourly average speed s (km/h).

116
117 Our FCD source covers France, Germany, and the Netherlands. Therefore, the 20 most populous cities within these three
118 countries were selected to develop high-resolution emission maps. Table 1 shows the basic information (population, area, street
119 length, street density) of the 20 cities in 2023. Note that here Paris is the administrative city jurisdiction (Ville de Paris)
120 covering the central 20 arrondissements, so its area is much smaller than Berlin, which is both a city and a federal state.
121
122

123



Formatted: Font: (Asian) +Body Asian (宋体), (Asian) Chinese (Simplified, Mainland China)

Figure 1: Workflow of this study

139
140
141

Table 1: Information of 20 selected cities in 2023.

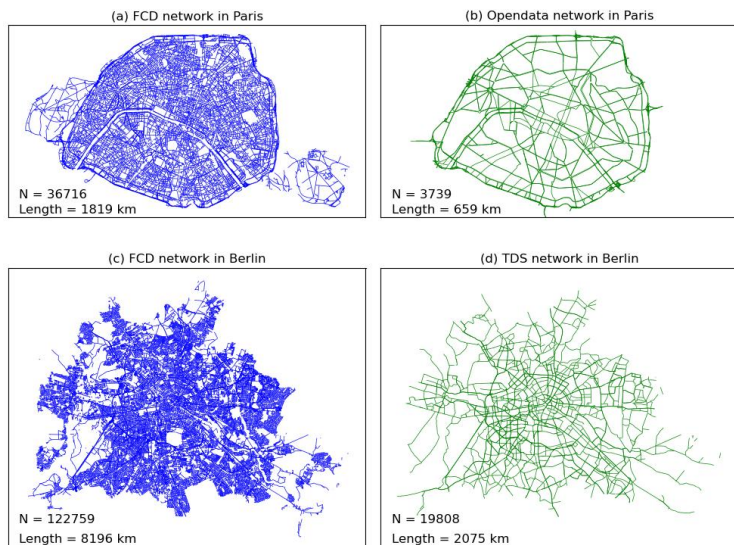
Country	City	Population (Thousand)	Area (km ²)	Street length (km)	Street density (km/km ²)
France	Paris	2,103	105.4	2412.9	22.9
	Marseille	862	240.6	3301.7	13.7
	Lyon	513	47.9	985.3	20.6
	Lille	233	39.5	679.8	17.2
	Toulouse	472	118.3	2311.2	19.5
	Nice	343	71.9	1228.0	17.1
	Nantes	303	65.2	1249.4	19.2
	Strasbourg	277	78.3	1252.4	16.0
	Montpellier	278	56.9	1260.1	22.1
	Bordeaux	250	49.4	967.9	19.6
Germany	Berlin	3,782	891.3	12073.4	13.5
	Hamburg	1,910	755.2	8725.2	11.6
	Munich	1,510	310.7	5220.0	16.8
	Cologne	1,087	405.2	5508.8	13.6
	Frankfurt	776	248.3	3648.5	14.7
	Stuttgart	633	207.3	3660.8	17.7
	Dusseldorf	631	217.4	2741.5	12.6
Netherland	Amsterdam	883	219.4	3203.8	14.6
	Rotterdam	656	324.1	3555.7	11.0
	The Hague	553	98.1	1796.8	18.3

Formatted Table

142

143 **2.2 Description and preparation of FCD**

144 FCD provides hourly average speed and sample counts for each street, with separate data for cars and trucks reporting GPS
145 data. The FCD is linked with high-resolution road network datasets that feature information such as road length, speed category,
146 road functional class, lane category, on more detailed and complete road networks than public traffic datasets based on sensors.
147 As shown in Figure 2, public datasets used by previous studies are only available for a few cities and provide hourly traffic
148 data for 3,739 road segments in Paris (Xavier Bonnemaizon 2024) and 19,808 segments in Berlin (Anjos and Meier, 2025),
149 respectively. In contrast, FCD gives vehicle count samples and speed information for 36,716 roads in Paris and 122,759 roads
150 in Berlin, dividing long roads into more segments and encompassing a much greater number of small roads than the city-level
151 public datasets. All road segments were categorized into major, middle, and small according to the functional class defined by
152 the FCD. Major roads represent roads connecting major metropolitan areas, middle roads represent roads connecting
153 neighbourhoods, and small roads represent low-volume roads.



154
155 **Figure 2: Monitored road networks in this study and other public datasets in Paris and Berlin.** N represents the number of road
156 segments. (a) and (c) represent road networks from FCD for Paris and Berlin, respectively; (b) and (d) represent networks from Open Data
157 in Paris and Traffic Detection Systems in Berlin.

158
159 Missing values exist in the FCD due to unstable GPS signals, especially for small roads. The average data coverage of GPS
160 cars on major, middle, and small roads ranges from 67.0% - 97.7%, 40.4% - 93.8%, and 6.1% - 37.7%, respectively (Figure

161 S1a). The average data coverage of trucks is lower, ranging from 32.2% - 75.8%, 32.1% - 85.3%, and 1.8% - 32.2%,
162 respectively (Figure S1b). Machine learning was used here to fill data gaps, as the use of machine learning techniques has
163 shown great potential for both temporal and spatial imputation of missing data to reconstruct the full volume of traffic(Wen et
164 al., 2022). Eight features were chosen as predictors (Table 2) to train models. Temporal features (hour, day of the week, and
165 month) were used to capture diurnal and seasonal patterns in traffic behaviour. Observed road-specific daily mean traffic
166 counts and speeds [derived from hourly averages](#) were also used as indicators of baseline traffic intensity. Holiday indicators,
167 including school and public holidays, were included to account for potential shifts in travel demand. Finally, road
168 characteristics including speed category, functional class, and lane category were used to describe the physical and functional
169 attributes of each road segment.

170
171 **Table 2: Spatial-temporal features used as predictors of traffic variables**

Category	Features	Usage
Time	Hour, Day of week, Month	Diel and seasonal pattern
Road-specific traffic counts/speed	Daily mean derived from hourly averages	Baseline traffic intensity
Holiday	School holiday, Public holiday	Potential shifts in travel demand
Road characteristics	Speed category, Functional class, Lane category	Road capacity and flow characteristics

Formatted: Font: 小五, Font color: Black

Formatted: Space After: 10 pt, Line spacing: single, Border: Top: (No border), Bottom: (No border), Left: (No border), Right: (No border), Between : (No border)

Formatted Table

172
173 The full-year dataset was partitioned into two temporally isolated subsets: January-June (H1) and July-December (H2) due to
174 the large-scale dataset. Separate machine learning models were developed for each six-month interval, both incorporating
175 consistent feature engineering protocols for vehicle type differentiation (Cars and Trucks) and road classification. Model
176 training was conducted on 80% of the available data, with the remaining 20% held out as an independent test set to evaluate

177 generalization performance. Random forest (RF) and lightGBM models were tested for Paris to compare their performances.
178 As shown in Table S1, Random Forest (RF) and LightGBM exhibited comparable predictive performance across different
179 vehicle types, road types, and target variables (i.e., vehicle count and speed) but LightGBM required significantly less
180 computational time. In some cases, the efficiency gain is more than 10-fold e.g., to fill gaps of car count on major roads takes
181 6.25 s for LightGBM vs. 122.53 s for RF. This efficiency gain stems from LightGBM's histogram-based decision tree
182 learning and its leaf-wise tree growth strategy with depth constraints, which together enable faster training and better scalability,
183 especially for large datasets with continuous features. Given its high accuracy and computational efficiency, ~~we selected~~
184 LightGBM was chosen as the preferred model and trained individually for each of the 20 cities.
185

186 [The LightGBM validation performance is summarized in Table 3 using mean R², RMSE, and MAE across cities and road](#)
187 [classes, while the full city-level validation results are reported in Table S2. The LightGBM validation results are shown in](#)
188 [Table S2. 5-fold cross-validation results which aimed at evaluating the robustness of the model are presented in Table S3.](#)

Formatted: Not Highlight

189 Overall, the model demonstrates strong predictive performance across different vehicle types and target variables. For car
190 count, performance is consistently high on major roads, with R^2 values typically above 0.90 and reaching up to 0.97 (e.g., The
191 Hague and Amsterdam). On middle and small roads, R^2 varies between 0.53 and 0.85, and lower values are often observed in
192 cities with smaller datasets, such as Lyon and Nice, suggesting that data volume plays a critical role in model accuracy (Figure
193 S2). For car speed, the model also performs well on major roads R^2 (0.85-0.95) but shows greater variability on smaller roads,
194 where R^2 drops to as low as 0.39 in some cases (e.g., Paris or Lyon). The results of trucks are similar to those of cars, but with
195 slightly lower overall performance. Shapley values, a concept from cooperative game theory, are widely used to explain feature
196 importance in machine learning. This study used the Python package SHAP to estimate Shapley values applied to the model's
197 conditional expectation function (SHAP, 2025), revealing that the daily mean count and hour of day are the most influential
198 predictors, followed by day of week, road class, and month (Figure S3). High traffic volumes are associated with increased
199 model output, while hourly effects vary by time of day. In contrast, features such as lane type and school holidays show limited
200 influence.
201
202
203
204
205
206
207
208
209
210

Table 3: Summary of LightGBM validation performance across cities and road classes.

<u>Vehicle</u>	<u>Item</u>	<u>Road class</u>	<u>Mean R²</u>	<u>Mean RMSE</u>	<u>Mean MAE</u>
Car	<u>COUNT</u>	<u>Major</u>	<u>0.93</u>	<u>16.34</u>	<u>9.08</u>
Car	<u>COUNT</u>	<u>Middle</u>	<u>0.73</u>	<u>6.09</u>	<u>3.91</u>
Car	<u>COUNT</u>	<u>Small</u>	<u>0.60</u>	<u>3.66</u>	<u>2.15</u>
Truck	<u>COUNT</u>	<u>Major</u>	<u>0.78</u>	<u>3.31</u>	<u>2.00</u>
Truck	<u>COUNT</u>	<u>Middle</u>	<u>0.57</u>	<u>1.88</u>	<u>1.29</u>
Truck	<u>COUNT</u>	<u>Small</u>	<u>0.54</u>	<u>1.87</u>	<u>1.15</u>
Car	<u>SPEED</u>	<u>Major</u>	<u>0.89</u>	<u>6.72</u>	<u>4.64</u>
Car	<u>SPEED</u>	<u>Middle</u>	<u>0.67</u>	<u>6.71</u>	<u>4.87</u>
Car	<u>SPEED</u>	<u>Small</u>	<u>0.58</u>	<u>7.85</u>	<u>5.63</u>
Truck	<u>SPEED</u>	<u>Major</u>	<u>0.84</u>	<u>8.77</u>	<u>6.35</u>
Truck	<u>SPEED</u>	<u>Middle</u>	<u>0.55</u>	<u>7.81</u>	<u>5.85</u>
Truck	<u>SPEED</u>	<u>Small</u>	<u>0.56</u>	<u>7.70</u>	<u>5.65</u>

2.32 Obtain CO₂ emission factors using COPERT

To calculate the speed-dependent emission factors EF_{CO_2} defined by CO_2 emissions per km driven for each vehicle type, we applied the COPERT model, a widely used emissions calculator for vehicles in Europe (Ntziachristos et al., 2009). Monthly temperature and relative humidity data required as input for COPERT were obtained from ERA5 reanalysis (Hersbach, 2023) and interpolated to a 0.01° spatial resolution. City-level averages of maximum/minimum temperature and relative humidity were then calculated within administrative boundaries defined by Eurostat shapefiles to serve as inputs for COPERT.⁵ Considering the data scale and time cost, instead of running COPERT for each street segment each hour, this study developed fitting curves between speed and EF_{CO_2} to obtain EF_{CO_2} . Except for L-Category vehicles running on diesel, where COPERT provides a fixed value, emission factors were simulated for various vehicle types at speeds of 20, 40, 60, 80, 100, 120, and 140 km/h. Then, for each city, cubic functions were fitted to COPERT simulations, as given by:

$$EF \equiv a \times s^3 + b \times s^2 + c \times s + d \quad (2)$$

229 Where s represents the average speed at hourly resolution, and aa , bb , ce , and d are city-specific constants. Table S43 presents
230 the parameters of the curve fitting results for all cities, showing a good fit quality with an R^2 value range from 0.882 to 0.998.
231 In this way, the corresponding emission factor for any given speed can be determined. Note that we used EF_{CO_2} of the EU6
232 standard, since CO_2 emission factors are only marginally influenced by emission standards, and this approach was also adopted
233 by TomTom (Index, 2024).

235 2.3.4 Estimate real traffic volume from sample count

236 Road-specific hourly total traffic volume is the key parameter to estimate CO_2 emissions. Since not all vehicles transmit GPS
237 signals and our dataset only captures a subset of the real GPS data for all vehicles, the actual traffic volume is significantly
238 higher than the sample counts from the FCD. To solve this problem, we established a relationship between real traffic volume
239 data and GPS sample count using machine learning. Due to the availability of traffic volume data, only the Opendata from
240 Paris (Parisopendata, 2024) and Traffic detection Berlin (Berlinopendata, 2024) were used for modelling. Opendata from Paris
241 provides hourly total vehicle flow from permanent sensors with electromagnetic loops on 2086-2278 roads in 2023, but does
242 not differentiate between vehicle types for the traffic volume. Therefore, the numbers of cars and trucks are estimated based
243 on the proportion of sample counts from each type in our FCD. Traffic detection in Berlin provides hourly total vehicle volumes
244 on 231 roads, and only the volumes of cars were used for modelling. As shown in Figure 2, monitored road networks of public
245 datasets and FCD are different. The overlap rate and angle are used as criteria to link the two datasets' shapefiles (Figure S4).
246 When the overlap rate > 0.7 and the angle $< 20^\circ$, a road is identified as being the same in Opendata and FCD. In this way,
247 hourly open data from 2278 monitoring sites in Paris and 231 monitoring sites in Berlin were matched to the FCD, and we got
248 the real volume and the number of FCD sample counts on the same road. A similar set of predictors as listed in Table 2, except
249 for road-specific traffic counts and speeds, was used to build a LightGBM model to extrapolate FCD sample counts to total
250 traffic volume. For cars in German cities, we used the LightGBM model trained on Berlin's data, while for all other cities, we
251 used the LightGBM trained on Paris's data. The results of validation are shown in Table S4. The validation results (Table
252 S4S5) show that the LightGBM model performs well on major roads in both Paris ($R^2 = 0.91$ for cars and 0.88 for trucks) and
253 Berlin ($R^2 = 0.66$ for cars). The accuracy decreases on middle and small roads in Paris (R^2 range from 0.22 to 0.38), while the
254 performance in Berlin remains comparatively good (R^2 range from 0.86 to 0.88). 5-fold cross-validation results are presented
255 in Table S6.

256
257 (Bonnemaizon et al., 2025) In addition to Paris and Berlin that are used for model training, observed traffic-count-based annual
258 average daily traffic flow (AADT, in number of vehicles per day) or annual average weekday traffic (AAWT, equivalent to
259 AADT excluding weekends) datasets are available for six additional cities reported in a recent study (Bonnemaizon et al., 2025):
260 Montpellier and Hamburg (AADT), and Bordeaux, Lyon, Toulouse and Lille (AAWT). The comparison which serves as
261 independent external validation to assess our traffic volume estimates is shown in Figure 3. Paris, the most important reference

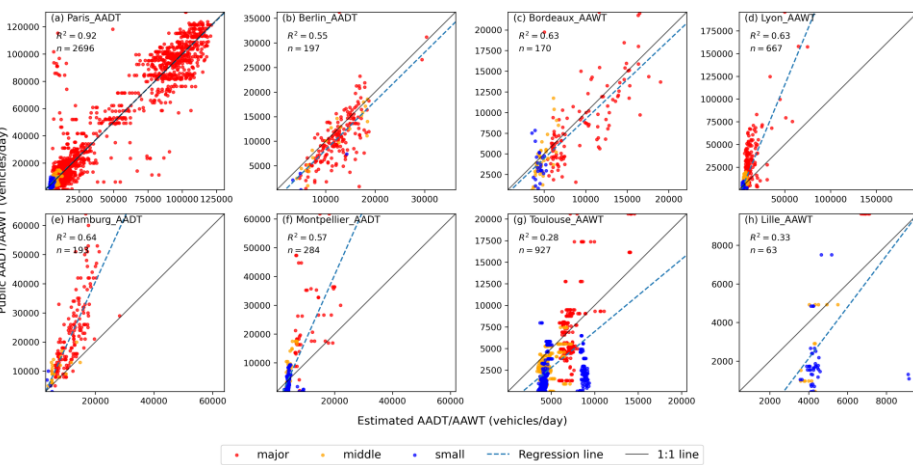
Formatted: Font: (Asian) Times New Roman, Not Highlight

Formatted: Font: (Asian) Times New Roman

Formatted: Not Highlight

262 city for model development, shows strong agreement between estimated and public AADT values ($R^2 = 0.92$, $n = 2696$), with
263 data points across all road classes closely aligned with the 1:1 line. Berlin exhibits noticeably larger dispersion, with a moderate
264 R^2 (0.55) derived from a relatively small sample size ($n = 197$), which likely contributes to the lower correlation.
265

266 Lyon, Hamburg, Bordeaux and Montpellier all show moderate correlation (with R^2 around 0.6). However, while simulated and
267 observed traffic volumes are generally well aligned for Bordeaux, public observations for Lyon, Hamburg and Montpellier
268 tend to exceed the simulated values, especially for the major roads. Toulouse and Lille are characterized by low correlation
269 (R^2 around 0.3), exhibits the weakest consistency between estimated and public traffic volumes. Overall, the scatter plots reveal
270 pronounced city-to-city heterogeneity in traffic volume agreement, providing important context for subsequent uncertainty
271 propagation to city-scale emission estimates.
272



273
274 **Figure 3: Comparison of AADT/AAWT between this study and public datasets.**
275

276 **2.4.5 Fleet structure**

277 This study collected fleet structures data in 2023 for the 20 cities to further map cars and trucks to 5 categories (passenger cars,
278 light commercial vehicles, buses, L-category and heavy-duty trucks), and 12 sub-categories, 10 fuels (petrol, diesel, CNG,
279 diesel hybrid, biodiesel, diesel PHEV, CNG biofuel, petrol hybrid, battery electric) [- as shown in Table 4 \(Table S5\)](#). The data

Formatted: Font: (Asian) Times New Roman, 小五, Bold, Font color: Black, English (United Kingdom)

Formatted: Font: (Asian) Times New Roman, Bold, English (United Kingdom)

Formatted: Justified, Space After: 10 pt, Line spacing: single, Border: Top: (No border), Bottom: (No border), Left: (No border), Right: (No border), Between : (No border)

Formatted: Font: (Asian) +Body Asian (宋体), (Asian) Chinese (Simplified, Mainland China)

280 that is reported annually was collected from the official statistical websites of France, Germany, and the Netherlands (Table
281 S76). Only direct emissions from fossil fuels are considered, so the emission factor of battery electric cars is set to 0.

288 **Table 4: Vehicle categories**

<u>Big Category</u>	<u>Category</u>	<u>Fuel</u>
Car	<u>L-Category</u>	Petrol, Diesel
	<u>Buses</u>	Petrol, Diesel, CNG, Diesel Hybrid, Biodiesel, Battery electric, Diesel PHEV
	<u>Passenger Cars</u>	Petrol, Diesel, CNG, Petrol Hybrid, Petrol PHEV, Battery electric, Diesel PHEV
Truck	<u>Heavy Duty Trucks</u>	Petrol, Diesel, Diesel PHEV, Battery electric, CNG
	<u>Light Commercial Vehicles</u>	Diesel, Petrol, Diesel PHEV, Battery electric, CNG, Petrol Hybrid, Petrol PHEV

291 **2.5.6 Aggregation onto grids**

292 Python was used to map street network emissions data onto a 100×100 m grid. Starting from a shapefile containing road
293 segments with associated emissions, a spatial join was performed using GeoPandas' sjoin function to identify which road
294 segments intersect each grid cell. Emissions were then allocated to the grid cells in a length-weighted manner, proportionally
295 distributing each road segment's emissions based on the length of its overlap with each cell. For the projections, cities in
296 France use EPSG:2154, while most German cities use EPSG:25832; Berlin uses EPSG:25833 due to its location. Dutch cities
297 are projected using EPSG:28992.

298 Formatted: Font: (Asian) Times New Roman, 小五, Bold, Font color: Black

Formatted: Font: (Asian) Times New Roman, 小五, Font color: Black

Formatted: Font: (Asian) Times New Roman, 小五, Bold, Font color: Black

Formatted: Space After: 10 pt, Line spacing: single, Border: Top: (No border), Bottom: (No border), Left: (No border), Right: (No border), Between : (No border)

Formatted Table

Formatted: Font: (Asian) +Body Asian (宋体), (Asian) Chinese (Simplified, Mainland China)

Formatted: Font: (Asian) +Body Asian (宋体), (Asian) Chinese (Simplified, Mainland China)

Formatted: Normal

299 [2.7 Uncertainty analysis](#)

Formatted: Font: (Asian) +Body Asian (宋体), (Asian) Chinese (Simplified, Mainland China)

300 Monte Carlo method is widely used in emission studies to estimate uncertainties (Ramírez et al., 2008; Zhao et al., 2011; Super et al., 2020). To quantify the uncertainty in estimated annual emissions arising from uncertainty in traffic volume estimates, this study applied a Monte Carlo simulation framework that propagates the observed discrepancies between estimated traffic volumes and public AADT/AAWT datasets (Figure 3) to the city-scale emission. Because emissions are linearly proportional to traffic volume, uncertainty in traffic counts can be directly transferred to emission uncertainty. As standard parametric assumptions (e.g., lognormality) did not adequately describe the tails of the discrepancy distributions, this study adopted a fully empirical cumulative distribution function (ECDF) approach. Discrepancy ratios were grouped by functional road class (major, middle, and small). For the six cities with observed AADT/AAWT data (Paris, Berlin, Bordeaux, Lyon, Hamburg, Montpellier, Toulouse and Lille), discrepancy ratios were sampled directly from the city-specific ECDFs. For cities without observations, we used country-level pools: ratios for French cities were sampled from the pool formed by the observed French cities, ratios for German cities from the observed German cities, and ratios for Dutch cities from a combined pool of the observed French and German cities.

312
313 For each Monte Carlo iteration j , the set of ratio values corresponding to a given road class was selected. A random value $u \sim$
314 $U(0,1)$ was drawn, and the corresponding correction factor was obtained via quantile sampling from the empirical distribution,
315 $F_R^{-1}(u)$. The total city-scale emissions for iteration j were then computed as:

$$319 \quad T_j = \sum_i E_i \times F_R^{-1}(u)$$

320 where E_i represents the baseline annual emissions of road link i , and the sampled correction factor was consistently applied to
321 all links within the same road class. This process was repeated 10,000 times ($j = 1, \dots, 10,000$), yielding a full ensemble of
322 possible emission totals. From the resulting Monte Carlo ensemble, 95% confidence interval was calculated.

Formatted: English (United States)

323 **3 Results**

324 **3.1 Annual emissions**

325 The total on-road CO₂ emissions in 2023 among the 20 cities ranged from 0.4 Mt CO₂/yr to 7.9 Mt CO₂/yr. The top five emitting cities are Berlin (7.9 Mt), Hamburg (6.6 Mt), Cologne (4.1 Mt), Munich (3.5 Mt), and Rotterdam (3.0 Mt). Berlin's CO₂ emissions are approximately 20 times higher than those of Lille, the city with the lowest emissions in the dataset (0.4 Mt). On average, the 20 cities emit 2.4 Mt CO₂ per year, with a coefficient of variation of 0.82 (Figure 43a). As shown in Figure 54, the linear regression analyses between on-road CO₂ emissions and both urban area and population indicate strong positive relationships. Specifically, CO₂ emissions increase significantly with larger urban areas and higher population sizes. The

329 regression model yields a high coefficient of determination with an R^2 value of 0.98 when emissions are regressed against area,
330 suggesting that urban land extent is a dominant factor influencing total emissions. A similarly positive but weaker correlation
331 is observed between emissions and population, with an R^2 value of 0.74, indicating that population size also plays a substantial
332 role in shaping emission levels. This distinction is further illustrated by a comparison between Paris and Hamburg. While their
333 populations are relatively similar, Hamburg covers an urban area nearly seven times larger than that of central Paris.
334 Furthermore, Hamburg's road network is more than three times as long. As a result, Hamburg exhibits substantially higher on-
335 road CO₂ emissions, reinforcing the observation that urban spatial extent and infrastructure scale are critical determinants of
336 total emissions, potentially more so than population alone.

337

338 [Table S8](#) compares the annual emissions estimated in this study with those reported by Carbon Monitor and other available
339 data sources. Carbon Monitor provides $0.1^\circ \times 0.1^\circ$ daily gridded maps named GRACED (Dou et al., 2023). City boundaries
340 were applied to clip GRACED grids, and area-weighted daily emissions were aggregated to annual city-level totals. Available
341 data of several cities from Climate Trace (Kott et al., 2024), local statistical websites (Bilanz des Statistikamtes Nord, 2024),
342 and previous studies (Kühbacher et al., 2023; Ulrich et al., 2023; Anjos and Meier, 2025) was also collected. Overall, estimates
343 of other datasets are much lower than this study, with differences ranging from -94.2% (Nice, Carbon Monitor) to -8.1%
344 (Berlin, Ulrich et al.'s estimates from Opendata) relative to our estimates. These discrepancies can be explained by the methods
345 of different datasets. Compared with local statistical reports, our estimates tend to be higher because we include emissions
346 from vehicles traveling across city boundaries, whereas local statistics typically estimate emissions based only on oil
347 consumption within administrative limits. GRACED allocates emissions based on EDGARv5 using OpenStreetMap data
348 without actual traffic volume data, this method likely underestimates emissions in large cities with high-volume roads. Climate
349 Trace estimates average annual daily traffic (AADT) by integrating Sentinel-2 satellite imagery with AADT data from the U.S.
350 Department of Transportation's Federal Highway Administration (FHWA), applying Convolutional Neural Network and
351 Graph Neural Network models. This U.S.-centric training may limit the models' applicability in the European context. Finally,
352 although our approach benefits from a more comprehensive road network, the relatively low accuracy on middle and small
353 roads may contribute to overestimation of traffic volumes in certain areas, as mentioned in Section 2.4.

354

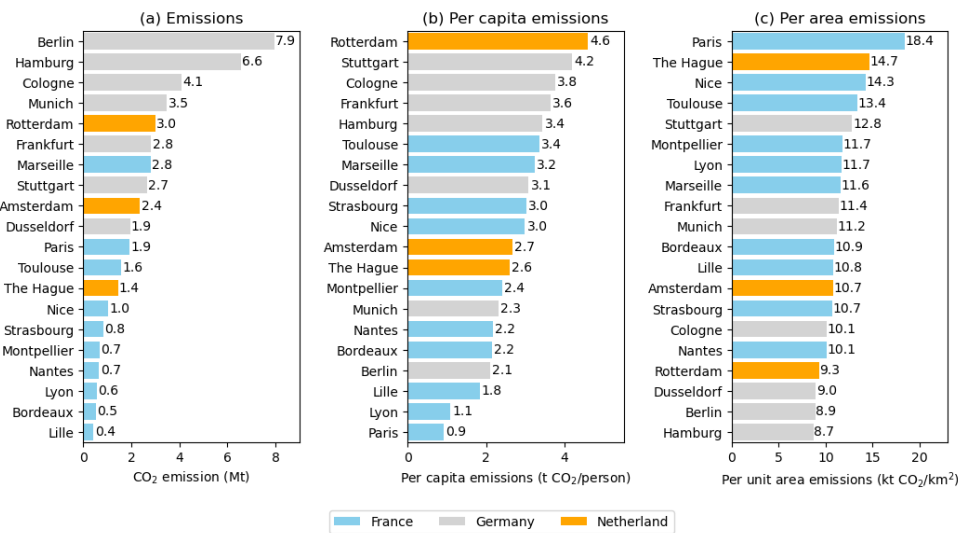
355

356 Per capita emissions show a mean of 2.8 tons/person with a coefficient of variation of 0.4, and the ranking is quite different
357 from total emissions (Figure 3b4b). Some of the cities with high total emissions also have high per capita emissions, such as
358 Cologne (3.8 t/person), Rotterdam (4.6 tons/person) and Frankfurt (3.6 tons/person). Other cities like Berlin (2.1 t/person) and
359 Paris (0.9 t/person) exhibit low per capita values despite their large total emissions. Notably, cities such as Toulouse (3.4
360 tons/person) and Marseille (3.2 tons/person) have high per capita emissions, highlighting differences in cities' boundaries e.g.,
361 including or not satellite towns commuting with each 'city', transportation infrastructure, commuting patterns, and vehicle
362 efficiency across the regions. Figure 3e-4c illustrates the emissions per unit area, revealing a contrasting pattern to total

Formatted: Font: (Asian) +Body Asian (宋体), (Asian) Chinese
(Simplified, Mainland China)

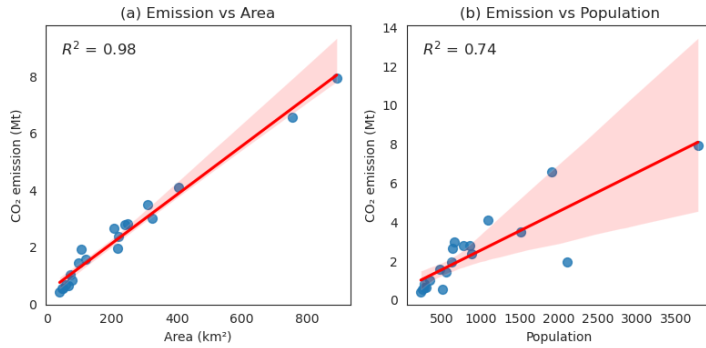
363 emissions. Paris exhibits the highest emissions per unit area ($0.02 \text{ Mt}/\text{km}^2$), despite having one of the lowest per capita values,
 364 which is indicative of its dense urban environment and intensive transportation activities within a compact city layout and a
 365 very dense street network. Similarly, Toulouse ranks second in per-area emissions, despite being only seventh in total
 366 emissions. This result shows that urban density and mobility intensity significantly influence emission distribution at the local
 367 scale.

368



369
 370 **Figure 34:** Annual CO₂ emission and emission intensities per capita and per unit area of 20 cities in 2023. Grey, light blue and orange
 371 represent cities in Germany, France and the Netherlands, respectively.

372



373
374 **Figure 45:** Linear relationships between on-road CO₂ emissions, area, and population. Each point represents one city.
375

376 3.2 Spatial patterns

377 Figure 5-6 presents the annual emission maps for 20 major European cities, highlighting the diversity in emission spatial
378 patterns. In addition, two cities from each country were selected to plot cumulative emission curves, as shown in Figure S5. In
379 cities such as Paris, Amsterdam, The Hague and Dusseldorf, a few major roadways stand out significantly in bright yellow. In
380 Paris, the top 5% of the highest-emitting 100 m grids contribute 33.1% of total emissions. The ring road known as le
381 Périmérique emerges as a major hotspot, accounting for 26.9% of the city's total on-road emissions and having a mean
382 emission level that is 953.3% higher than the city-wide average. This is primarily attributable to its high traffic density and
383 heavy vehicle usage driven by significant commuter flows. A similar concentration of emissions is observed in Amsterdam,
384 where the top 5% of the highest-emitting 100 m grids contribute 30.3% of total emissions, respectively, underscoring the
385 spatially skewed distribution of traffic-related CO₂. The top 5% of high-emission grids in The Hague and Dusseldorf show a
386 lower contribution of total emissions (24.5% and 21.9% respectively), but these are still concentrated along major highways
387 such as the A4 and A12 in The Hague and B8 and A44 in Dusseldorf. The steep curvatures at the start of the cumulative
388 emissions distribution curves for these two cities suggest that only a few key segments are disproportionately responsible for
389 emissions, albeit to a lesser extent than in Paris or Amsterdam.

390
391 Cities like Berlin and Bordeaux exhibit a more diffuse emission pattern, with relatively less pronounced hotspots, where the
392 top 5% of the highest-emitting 100 m grids contribute ~19.0% of total emissions. Their cumulative emission curves
393 demonstrate gentler slopes, indicating a more uniform spread of emissions across the road network. This suggests that no
394 single road or corridor dominates in terms of emission contributions and that urban transport emissions are more evenly
395 distributed. Other cities, including Lyon, Marseille, Frankfurt, and Rotterdam, fall between these two extremes, exhibiting

396 varying degrees of emission concentration. For instance, Frankfurt shows notable linear patterns corresponding to high-
397 emission highways intersecting the urban core. In contrast, Rotterdam reveals both concentrated and dispersed emission zones
398 due to its mixed land use and logistic traffic. Overall, these spatial variations emphasize the importance of city-specific
399 mitigation strategies. While targeted interventions on a few high-emitting corridors may yield significant benefits in cities with
400 highly skewed distributions (e.g., Paris or Dusseldorf), broader, network-wide policies may be necessary in more evenly
401 distributed urban contexts like Berlin or Bordeaux.

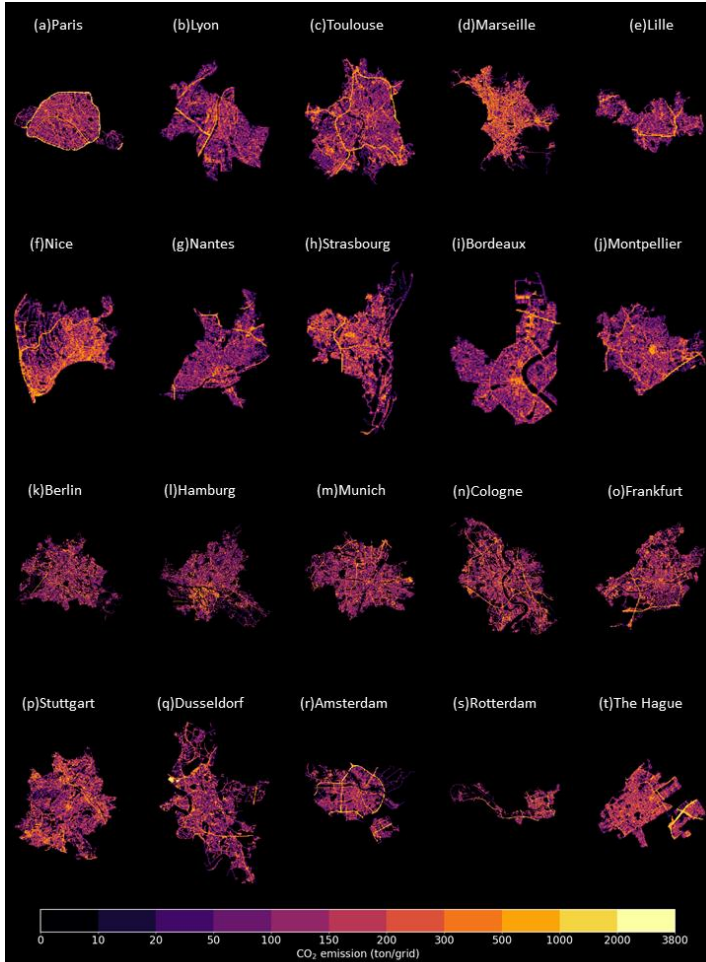


Figure 65: Annual CO₂ emission map of 20 cities at 100m × 100m resolution in 2023.

405 **3.3 Temporal patterns**

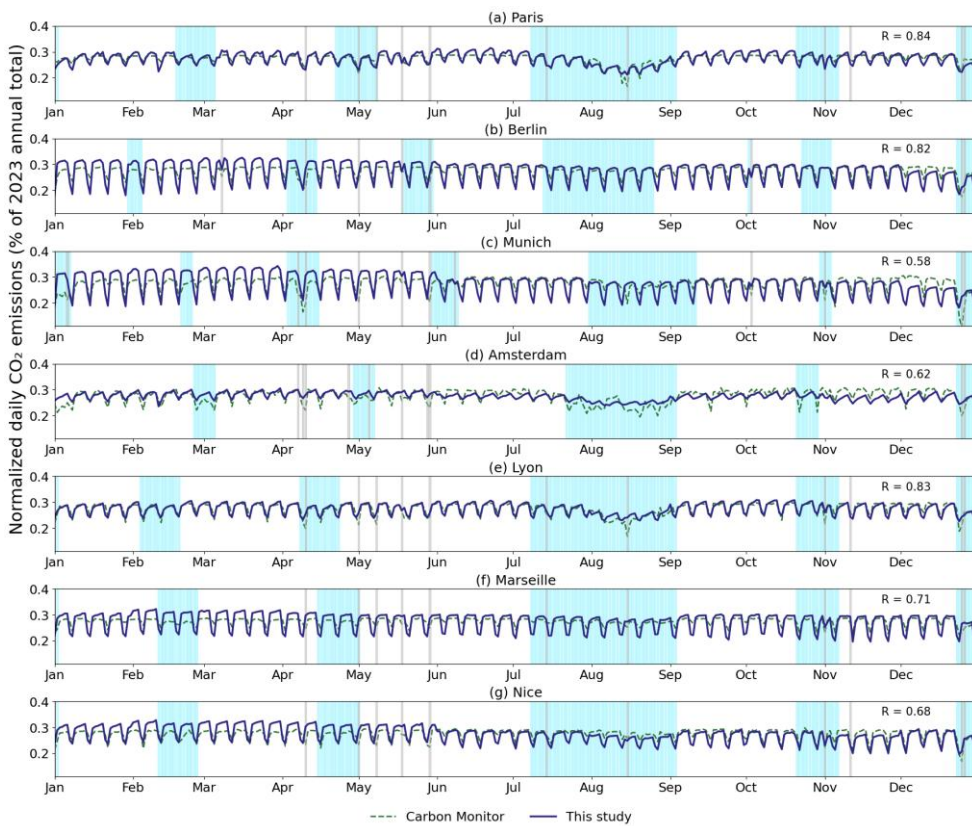
406 Figure 6-7 presents the normalized daily CO₂ emissions ratios for Paris, Berlin, Munich, Amsterdam, Lyon, Marseille, and
407 Nice in 2023. The y-axis represents each day's CO₂ emissions divided by the city's total emissions in 2023. These cities were
408 selected due to the availability of corresponding Carbon Monitor Cities data (hereafter CM-Cities data, shown as green dashed
409 lines), which enables direct comparison with the results of this study (blue lines). The time series data reveals distinct seasonal
410 and weekly variations. The summer months (July and August) show a significant decline in emissions in Paris, Amsterdam,
411 and Lyon, while emissions in all seven cities decline around Christmas, due to business closures and decreased commuting.
412 For weekly patterns, there is a slight upward trend from Monday to Friday, a noticeable drop on Saturday, and a further decline
413 on Sunday (Figure S6). The magnitude of the weekend drop varies across cities. In Berlin and Marseille, the median emissions
414 on Sunday drop by approximately 31.1% and 27.7% compared to Friday in 2023, respectively, representing the most
415 pronounced Sunday reduction among the six cities. In contrast, Amsterdam exhibits a much smaller Sunday drop compared to
416 Friday (10.1%).
417

Formatted: Font: (Asian) +Body Asian (宋体), (Asian) Chinese (Simplified, Mainland China)

418 In all cities, the median emissions of public holidays (marked in grey shades) and school holidays (marked in light blue shades)
419 are lower than those of weekdays in 2023. Across all six cities, the median emissions on public holidays and school holidays
420 were consistently lower than weekday levels in 2023, indicating a general reduction in traffic-related CO₂ emissions during
421 holiday periods. In Paris, public holiday emissions were exceptionally low, even lower than Sunday levels by 5.2%. The pattern
422 is different in Marseille, Berlin, and Nice, as the median emissions on public holidays exceeded those on Saturdays by 24.4%,
423 11.0%, and 6.4%, respectively. The medians of school holidays are generally higher than those of public holidays because a
424 more limited segment of the population is affected, and the distributions are notably wider. An exception is Amsterdam, where
425 public holiday emissions slightly surpassed those during school holidays, suggesting a different urban rhythm or school break
426 dynamics compared to other cities. Also, the day of the week on which a holiday falls also influences emission levels. As
427 shown in Figure S7, holidays that coincide with weekends tend to show similar emission levels to regular weekend days. When
428 holidays fall on a Monday, their emission levels are comparable to those of regular Mondays in cities like Berlin, Marseille,
429 and Nice.
430

431
432

Formatted: Font: (Asian) +Body Asian (宋体), (Asian) Chinese (Simplified, Mainland China)



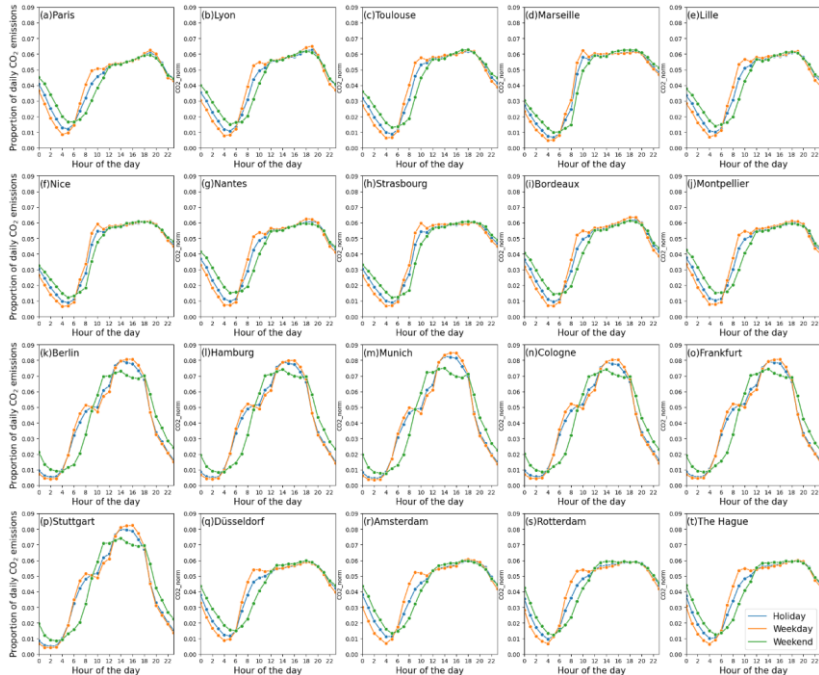
435 **Figure 7: N-6: Normalized daily CO₂ emission of seven cities in 2023.** Y-axis represents each day's CO₂ emissions divided by the city's
 436 total emissions in 2023. The light blue and grey shades represent school holidays and public holidays, respectively. The y-axis represents
 437 each day's CO₂ emissions divided by the city's total emissions in 2023.

438 Although the general emission temporal variability estimated in this study align reasonably with those reported by Carbon
 439 Monitor Cities, as evidenced by the R correlation coefficients ranging from 0.58 to 0.84 across the six selected cities, notable
 440 differences remain. In Paris, CM-cities tends to underestimate both the troughs and peaks of emissions (Huo et al., 2022). In
 441 Lyon, the consistency is relatively high, but the sharp weekend emission drops observed in Carbon Monitor estimates are not
 442 reproduced in this study. In Amsterdam, this study does not show the pronounced weekend decreases during holidays that are

443 present in Carbon Monitor data. CM-cities estimated traffic volumes using a sigmoid regression based on TomTom live
444 congestion indices, which lack spatial granularity (only one value per city), and the model parameters were calibrated using
445 real-time data from approximately 60 roads in Paris. In addition, CM-cities adopts the Functional Urban Area (FUA) definition
446 used by the OECD and the European Union, which includes high-density urban centers along with their surrounding
447 commuting zones, whereas our analysis relies on administrative boundaries. For cities not covered by CM-cities, we compared
448 daily emissions clipped from GRACED (Figure S8). Without calibration at the city level as CM-cities did, GRACED daily
449 emissions fail to show a consistent weekday–weekend pattern, and some anomalous peaks occurred (e.g., elevated emissions
450 in Hamburg in April 2023 and in Frankfurt and Montpellier in late May 2023). Except for The Hague, Rotterdam, and Bordeaux,
451 the resulting daily profiles showed very poor agreement ($R < 0.4$). These findings suggest that coarse-resolution data are not
452 suitable for city-level temporal analyses, highlighting the advantage of our city-scale dataset in more accurately representing
453 actual urban emissions.

454 ▲
455 Figure 7–8 presents the average hourly CO₂ emission patterns for cars across the 20 cities in 2023. The y-axis represents the
456 average proportion of daily CO₂ emissions for each hour, categorized by day types: holidays (blue), weekdays (orange), and
457 weekends (green). The hourly patterns for cars in French cities and Dutch cities are similar. On weekdays, there are two
458 emission peaks at 9:00~10:00 and 18:00~19:00 due to commuting, and the emissions stabilize at relatively high levels between
459 these two peaks. After the second emission peak, the emissions decline continuously and reach their lowest point at 4:00 ~
460 5:00. The differences between weekdays and holidays are relatively small, but with no or a less pronounced morning peak due
461 to reduced commuting activity. On weekends, the sum of average emission share in French cities and Dutch cities during
462 evening and early morning (22:00 to 6:00) reach 22.9% to 29.1%, significantly higher than that for weekdays (17.4 to 21.7%),
463 and the first peak is lagged to around 12:00. German cities on weekdays, except for Dusseldorf, the CO₂ emission exhibit
464 earlier morning peaks at 8:00 and a much higher peak around 15:00 ~16:00. On average, evening peak emissions in French
465 and Dutch cities are only around 15% higher than morning peak levels, but for German cities specifically, the difference ranges
466 from 9.3% to 60.0%. After the peak, the CO₂ emissions in German cities decrease sharply, which is consistent with the trends
467 reported by the Berlin datasets (Max et al). On weekends, there is only one peak around 13:00.

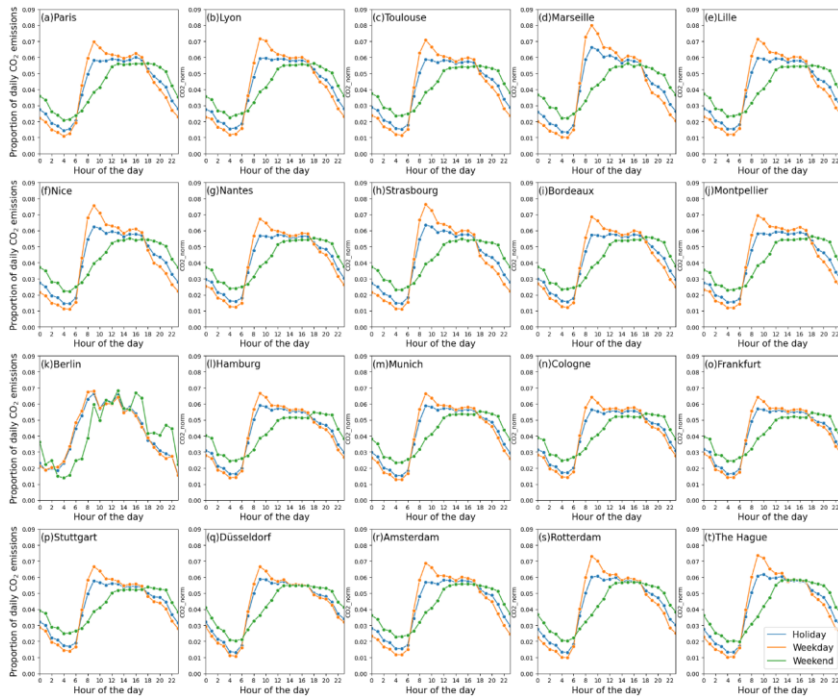
Formatted: Font: (Asian) +Body Asian (宋体), (Asian) Chinese (Simplified, Mainland China)



468
469 **Figure 78: Hourly emission patterns of cars in 20 cities.**

470

471 The hourly patterns for trucks are relatively consistent across all 20 European cities but are notably different from those of
 472 passenger cars (Figure 98). On weekdays, truck-related CO₂ emissions show a peak around 9:00 in nearly all cities, suggesting
 473 synchronized delivery and logistics activity. This peak accounts for 5.4%–6.5% of daily truck emissions in French and Dutch
 474 cities, and up to 9% in German cities such as Berlin and Hamburg. Truck emissions on weekends and holidays are considerably
 475 reduced, with no discernible peaks in most cities. In some German cities (e.g., Stuttgart and Düsseldorf), truck emissions
 476 remain below 3% of daily total at any hour during holidays, reflecting stricter weekend freight regulations. In contrast,
 477 emissions levels of trucks remain relatively high on weekends, especially in southern cities like Marseille and Nice, where
 478 midday peaks surpass 0.06 of daily emissions and are comparable to weekday levels.



479
480 **Figure 28:** Hourly emission patterns of trucks in 20 cities.

481
482 **3.4 Validation**

483 Table S7 compares the annual emissions estimated in this study with those reported by Carbon Monitor and other available
484 data sources. Carbon Monitor provides $0.1^\circ \times 0.1^\circ$ daily gridded maps named GRACED(Dou et al., 2023). City boundaries
485 were applied to clip GRACED grids, and area-weighted daily emissions were aggregated to annual city-level totals. Available
486 data of several cities from Climate Trace(Kott et al., 2024), local statistical websites(Bilanz des Statistikamtes Nord, 2024),
487 and previous studies(Kühbacher et al., 2023; Ulrich et al., 2023; Anjos and Meier, 2025) was also collected. Overall, estimates
488 of other datasets are much lower than this study, with differences ranging from -94.2% (Nice, Carbon Monitor) to -8.1%
489 (Berlin, Ulrich et al.'s estimates from Opendedata) relative to our estimates. These discrepancies can be explained by the methods
490 of different datasets. Compared with local statistical reports, our estimates tend to be higher because we include emissions

491 from vehicles traveling across city boundaries, whereas local statistics typically estimate emissions based only on oil
492 consumption within administrative limits. GRACED allocates emissions based on EDGARv5 using OpenStreetMap data
493 without actual traffic volume data, this method likely underestimates emissions in large cities with high volume roads. Climate
494 Trace estimates average annual daily traffic (AADT) by integrating Sentinel-2 satellite imagery with AADT data from the U.S.
495 Department of Transportation's Federal Highway Administration (FHWA), applying Convolutional Neural Network and
496 Graph Neural Network models. This U.S.-centric training may limit the models' applicability in the European context. Finally,
497 although our approach benefits from a more comprehensive road network, the relatively low accuracy on middle and small
498 roads may contribute to overestimation of traffic volumes in certain areas, as mentioned in Section 2.3.

499
500 For daily profiles, we have discussed the general consistencies and the notable differences between our estimates and those
501 from CM cities (Figure 6, Section 3.3). CM cities estimated traffic volumes using a sigmoid regression based on TomTom
502 live congestion indices, which lack spatial granularity (only one value per city), and the model parameters were calibrated
503 using real time data from approximately 60 roads in Paris. In addition, CM cities adopts the Functional Urban Area (FUA)
504 definition used by the OECD and the European Union, which includes high-density urban centers along with their surrounding
505 commuting zones, whereas our analysis relies on administrative boundaries. For cities not covered by CM cities, we compared
506 daily emissions clipped from GRACED (Figure S8). Without calibration at the city level as CM cities did, GRACED daily
507 emissions fail to show a consistent weekday-weekend pattern, and some anomalous peaks occurred (e.g., elevated emissions
508 in Hamburg in April 2023 and in Frankfurt and Montpellier in late May 2023). Except for The Hague, Rotterdam, and Bordeaux,
509 the resulting daily profiles showed very poor agreement ($R < 0.4$). These findings suggest that coarse-resolution data are not
510 suitable for city-level temporal analyses, highlighting the advantage of our city-scale dataset in more accurately representing
511 actual urban emissions.

513 3.4 Uncertainty analysis

514 Figure 10 shows the uncertainties in annual emissions arising from uncertainty in traffic volume estimates. Overall, the Monte
515 Carlo-derived mean emission estimates are close to the original deterministic estimates for most cities, with the Monte Carlo
516 means being on average 13.1% lower across the 20 cities. The differences between the Monte Carlo mean and the deterministic
517 estimate for Paris (-7.0%), Lyon (+7.3%), and Bordeaux (-13.4%) remain within $\pm 15\%$, indicating relatively stable estimates
518 despite uncertainty propagation. Noticeable differences are observed for Berlin (-41.4%), Hamburg (+61.4%), Marseille
519 (-41.2%), and Toulouse (-46.5%), where the differences between the Monte Carlo mean and the deterministic estimate exceed
520 40%.

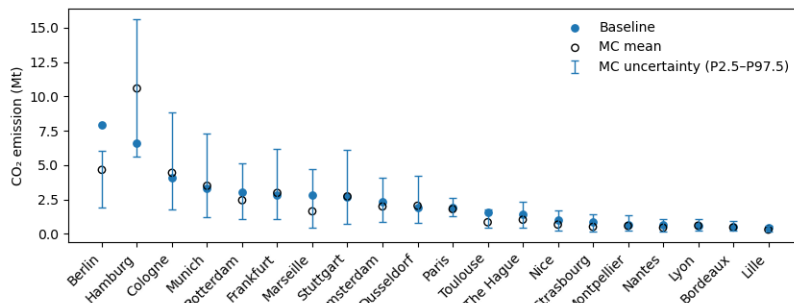
521
522 Figure S9 further shows the road-class-specific uncertainties. Across cities uncertainty in annual totals is primarily driven by
523 emissions associated with small roads, which exhibit the greatest relative variability across all functional classes. We quantify

524 road-class-specific relative uncertainty using the relative 95% interval width defined as $(P97.5-P2.5)/\text{mean}$ of the 10,000
525 Monte Carlo realizations. Using this metric, small roads show the largest relative uncertainty, with a median value of 2.67
526 (266.7%), compared with 1.74 (174.1%) for middle roads and 1.26 (125.8%) for major roads. In Berlin, the Monte Carlo
527 estimate is 4.65 Mt CO₂ (95% CI: [1.89, 6.04]), closer to values reported by Anjos et al (2.70 Mt) (Anjos and Meier, 2025) and
528 Climate Trace (1.99 Mt) (Kott et al., 2024), suggesting that the original deterministic estimate may have overestimated
529 emissions from small roads. The situation in Hamburg is different. The Monte Carlo mean emission estimate of approximately
530 10.57 Mt CO₂ (95% CI: [5.64, 15.60]) exceeds that of Berlin, which is unreasonable given Hamburg's smaller urban scale and
531 lower overall road lengths. This outcome suggests that limited and heterogeneous observational data can bias an upward bias
532 in the sampled correction factors for small roads, resulting in an overestimation of emissions for this road class and,
533 consequently, at the city scale.

Formatted: Subscript

534 Overall, these contrasting behaviours highlight that city-scale uncertainty is highly sensitive to the treatment of small roads,
535 particularly in data-scarce contexts. While the Monte Carlo framework provides a robust characterization of uncertainty, its
536 outcomes for low-traffic road classes should be interpreted with caution and ideally complemented by additional constraints
537 or external benchmarks.

Formatted: Justified



539
540 Figure 10: Emission uncertainties in 20 cities. Filled circles are the original deterministic estimates. Hollow circles indicate Monte
541 Carlo mean estimates, and vertical bars represent the 95% uncertainty interval (P2.5–P97.5).

Formatted: Left

Formatted: Font: (Default) Times New Roman

542 4 Discussion

543 4.1 Key contributions and implications

544 This study demonstrates that integrating new GPS-based traffic data for individual vehicles covering all street segments with
545 the COPERT model enables the estimation of hourly on-road CO₂ emissions at street level, which were further aggregated into
546 100 × 100 m grids for visualization display purposes, to generate high-resolution emission maps across 20 European cities.

Formatted: Font: (Asian) +Body Asian (宋体), (Asian) Chinese (Simplified, Mainland China)

Formatted: Heading 2

547 This approach overcomes the limitations of traditional top-down downscaling methods (e.g., population-based or road-network
548 density proxies) by applying machine learning to impute the actual traffic volumes from FCD, which only samples the traffic
549 of vehicles equipped with GPS. Compared to existing CO₂ emission inventories such as CAMS-TEMPO, Carbon Monitor, or
550 localized platforms [in Asian or German cities](#), our dataset represents a significant advancement by simultaneously achieving
551 high spatial granularity and temporal resolution. It captures intra-urban variability that is often missed in coarser-resolution
552 datasets or those relying solely on major road segments. This work highlights the value of integrating GPS-based mobility data
553 with machine learning and emission modelling to enhance the monitoring of urban transportation emissions and to inform the
554 design of effective, location-specific mitigation policies. Most [common](#) [current](#) low-carbon transport measures in cities
555 include modal shift to public transport, low-carbon zones control, and low-emission vehicle development, but each strategy
556 may vary according to development stages and types of urban land-use transport systems (Creutzig et al., 2012; Nakamura and
557 Hayashi, 2013; Croci et al., 2021). While low-density cities become more compact in the long term but often lack sufficient
558 population density to support rapid transit systems in the short term, promoting the adoption of electric vehicles, particularly
559 in regions with low-carbon electricity, may be a more practical approach (Kennedy et al., 2014). This study may support the
560 design of such strategies by enabling street-level scenarios to quantitatively assess their potential emission reductions.

561
562 Our [CO₂](#)-hourly [CO₂](#) emission maps reveal striking spatial heterogeneity within cities. For example, concentrated emission
563 hotspots along Paris' ring road, versus more dispersed patterns in Berlin, reflect differences in urban structure, transport
564 systems, and commuting behaviours. Temporally, we observed national variations in traffic-related emissions during holiday
565 and summer periods, likely due to country-specific vacation schedules. Our new emission maps can support planning of low-
566 emission zones, help identify high-flux corridors for targeted energy efficiency measures and provide a basis for congestion-
567 related studies. Given that traffic congestion is a major driver of both fuel consumption and emissions, our maps offer valuable
568 insights for designing and evaluating emission reduction strategies.

569

570 [4.2 Limitations](#)

571 Several sources of uncertainty remain in our approach. Because the GPS-to-volume conversion models were calibrated using
572 [in-situ](#) sensor data from Paris and Berlin only and extrapolated to the remaining 18 cities, the results may be better suited for
573 analysing spatial patterns, temporal dynamics, and relative differences across cities, rather than for precise reporting of absolute
574 emission magnitudes. To move beyond qualitative statements, we quantify activity-data uncertainty using independent annual
575 [AADT/AAWT](#) validation (Section 2.4; Figure 3) and Monte Carlo uncertainty propagation (Section 3.4; Figure 10 and Figure
576 59). The external validation reveals pronounced inter-city heterogeneity in traffic-volume agreement (with R² ranging from
577 approximately 0.3 to 0.92 across cities; Figure 3), which provides the empirical basis for the subsequent uncertainty ranges.

578

Formatted: Font: (Asian) +Body Asian (宋体), (Asian) Chinese (Simplified, Mainland China)

Formatted: Heading 2

579 First, significant uncertainty may be introduced during the conversion from GPS trajectories to actual traffic volume. The flux-
580 to-volume machine learning models were calibrated using sensor data from Paris and Berlin only, because comparable high-
581 resolution traffic counts are either unavailable or not publicly accessible for most other cities. In addition, GPS penetration
582 rates may vary across cities and vehicle types, and the vehicle population captured by FCD may differ from that represented
583 in local monitoring stations, which can affect calibration, particularly for trucks. As discussed in Sections 2.4 and 3.4, model
584 performance is weaker on middle and small roads, and emissions from small roads exhibit the largest uncertainty and potential
585 overestimation. Consistent with this, Monte Carlo mean emission estimates are on average 13.1% lower than the deterministic
586 totals across the 20 cities, and most cities remain within $\pm 15\%$. However, several cities show substantially larger deviations
587 exceeding 40% (e.g., Berlin, Hamburg, Marseille, and Toulouse), indicating that absolute totals are more uncertain where
588 traffic-volume discrepancies are large and observational constraints are limited. For example, Berlin's Monte Carlo estimate
589 is 4.65 Mt CO₂ (95% CI: [1.89, 6.04]), whereas Hamburg shows a much wider and higher range of 10.57 Mt CO₂ (95% CI:
590 [5.64, 15.60]), highlighting the sensitivity of city totals to correction factors on small roads in data-scarce contexts. This
591 reinforces the need for more comprehensive and standardized traffic monitoring networks. Incorporating additional top-down
592 constraints, such as city-level fuel consumption statistics in transportation sector, could further improve the accuracy of traffic
593 volume inference. However, several sources of uncertainty remain in our approach, primarily stemming from the FCD. First,
594 although we conducted extensive data cleaning, anomalies occasionally persist due to the instability and noise inherent in the
595 raw data. Second, there are uncertainties related to the GPS penetration rate. The proportion of vehicles equipped with GPS
596 devices may vary across vehicle types and cities. For instance, commercial vehicles are more likely to be tracked. This
597 discrepancy may lead to bias in estimating traffic volume from floating car data (FCD), particularly if the raw data or sensor-
598 based counts do not distinguish between vehicle categories. This study assumes that other cities have the same penetration
599 rates as Paris or Berlin, but if the other cities have lower penetrations, then their traffic volumes are underestimated. In such
600 cases, trucks may be overrepresented in the dataset, potentially leading to overestimation of freight-related emissions.

601
602 **Second** **Third**, uncertainties also arise from fleet structures. Due to the lack of detailed vehicle-type distribution at the road
603 segment level, we can only perform fleet correction for roads where heavy-duty vehicle traffic is explicitly restricted. For other
604 roads, we currently apply city-wide average fleet compositions, which may not reflect local variations. **Although urban fleet**
605 **structure evolves continuously, available data are reported at coarse temporal resolution; disaggregation to finer temporal**
606 **scales would introduce substantial uncertainty, and an annual fleet update is therefore adopted to maintain consistency with**
607 **the data and the emission modelling framework.**

608
609 Finally, emissions in this study are estimated using the COPERT, which is based on an average-speed framework and does not
610 explicitly represent microscopic stop-and-go driving behaviours. In contrast, microscopic emission models such as
611 MOVES(USEPA, 2024) explicitly account for such dynamics but require high-frequency trajectory data, which are not
612 available in this study. Moreover, COPERT characterizes vehicle technologies primarily by vehicle category and Euro

613 emission standard, and does not explicitly parameterize changes in emission performance associated with vehicle ageing. As
614 a result, city-specific fleet age structures and local real-world driving conditions may lead to deviations from the standard
615 emission factors used in the model, especially where detailed fleet data are unavailable to further refine the parameterization.
616 Access to locally measured emission factors from in situ studies or the literature would help reduce this source of uncertainty
617 and improve the accuracy of the emission estimates.

618 **4.3 Future work**

619 Finally, significant errors may be introduced during the conversion from GPS trajectories to actual traffic volume. Our
620 flux-to-volume machine learning models were calibrated using sensor data from Paris and Berlin only, as high-quality
621 in-situ traffic observations are either unavailable or not publicly accessible for other cities. As discussed in Section 3.4,
622 the models for middle and small roads in Paris still require further refinement for better performance. This limits the
623 models' generalizability and highlights the need for more comprehensive, standardized traffic monitoring networks.
624 Some traffic data from other cities are available at daily or annual resolutions (Bonnemaizon et al., 2025), and
625 integrating these in future work could support broader validation and model refinement. Also, the fleet captured by
626 FCD and local monitoring stations can be different. For example, utility vehicles are captured by FCD but not by the
627 Berlin Open-Data traffic counts, which could be the reason for the bad performance when we try to transform signals
628 to the real volumes for trucks. Incorporating additional top-down constraints, such as detailed fuel consumption data
629 could potentially improve the accuracy of this step.

630

631 Formatted: Font: (Asian) +Body Asian (宋体), (Asian) Chinese
(Simplified, Mainland China)

632 Formatted: Heading 2

633 Current work only covers the year 2023, but the underlying GPS-based FCD is typically available with a delay of only about
634 one week. This creates a clear opportunity to automate the processing pipeline and update the emission estimates on a rolling
635 basis. Incorporating this capability into Carbon Monitor Cities would allow near-real-time, high-resolution emission
636 monitoring at the street level, significantly enhancing the system's responsiveness and value for both research and policy
637 applications. In addition, further feature engineering could improve model performance. As part of ongoing work, we plan to
638 incorporate high-resolution urban context information, such as building-type data, to better capture heterogeneity across
639 different road classes. The proposed framework is flexible and allows additional features to be integrated as new data become
640 available. Also, future work could extend the methodology to include major air pollutants beyond CO₂ and scale the
641 approach to cover broader regions. Through incorporating more sensor-based traffic measurements across cities, data
642 representativeness and model validation can be further improved. Such efforts will strengthen the robustness, applicability,
643 and policy relevance of street-level emission mapping, particularly in supporting timely decision-making and climate or clean
air action monitoring.

644 **5 Data availability**

645 The high-resolution hourly CO₂ emission dataset for 20 cities in 2023 is available in NetCDF format, on Zenodo
<https://doi.org/10.5281/zenodo.16600210> (Shi et al., 2025). Each city has an individual NetCDF file that provides gridded

646 hourly emissions over the entire year of 2023. Their central x and y coordinates define the grid cells, and each file includes the
647 variable CO2_g, representing emissions in grams per hour in the grid. Every grid's size is 100 m × 100 m.

648 **Supplement**

649 This dataset is accompanied by Supplementary Information, including a detailed methodology document (SI_document.docx)
650 and additional data tables (SI_tables.xlsx).

651 **Author contributions**

652 QS processed and generated the dataset and drafted the initial manuscript. PC designed the study and provided scientific
653 supervision. NM collected the raw data and contributed to the structuring of the dataset. XB and RTM assisted with COPERT
654 data handling, data matching, and emission calculations. RE reviewed the emission estimates and provided constructive
655 feedback on the manuscript. CZ contributed extensively to the machine learning modelling and provided valuable suggestions
656 on the manuscript structure and visualization. All authors reviewed and approved the final manuscript.

657 **Competing interests**

658 The authors declare that they have no conflict of interest.

659 **Acknowledgement**

660 This study is funded by the Copernicus Atmosphere Monitoring Service (under the CAMS2_51a contract), which is
661 implemented by the European Centre for Medium-Range Weather Forecasts (ECMWF) on behalf of the European Commission.

662 **References**

663 Albarus, I., Lauvaux, T., Utard, H., Ciais, P., Crifo, P., and Gros, V.: Unraveling climate targets across the Paris conurbation
664 as a gauge of city ambitions, *npj Urban Sustainability*, 5, 27, 10.1038/s42949-025-00206-y, 2025.
665 Amsterdam, T. C. o.: Roadmap Amsterdam Climate Neutral 2050, 2024.
666 Anjos, M. and Meier, F.: Zooming into Berlin: tracking street-scale CO2 emissions based on high-resolution traffic modeling
667 using machine learning, *Frontiers in Environmental Science*, 12, 10.3389/fenvs.2024.1461656, 2025.
668 Verkehrsdetektion Berlin: <https://daten.berlin.de/datasets/verkehrsdetektion-berlin>, last access: 28/07/2025.
669 Erneut deutliche CO2-Minderung in Hamburg: [https://www.hamburg.de/politik-und-
670 verwaltung/behoeften/bukea/themen/klima/klimaschutz-klimaplan/co2-bilanz-hh-2023-169240](https://www.hamburg.de/politik-und-verwaltung/behoeften/bukea/themen/klima/klimaschutz-klimaplan/co2-bilanz-hh-2023-169240), last access: 28/07/2025.
671 Bonnemaizon, X., Ciais, P., Zhou, C., Shi, Q., Mittakola, R. T., Goldmann, C., Ben Arous, S., Megel, N., and Davis, S. J.:
672 Harmonized Annual Averaged Traffic Data at Street Segment Level for European Cities, *Scientific Data*, 12, 1365,
673 10.1038/s41597-025-05698-y, 2025.

674 E-Mobility revolution in Amsterdam: https://cinea.ec.europa.eu/news-events/news/e-mobility-revolution-amsterdam-2025-04-23_en?utm_source=chatgpt.com, last access: 28/07/2025.
675
676 Creutzig, F., Mühlhoff, R., and Römer, J.: Decarbonizing urban transport in European cities: four cases show possibly high
677 co-benefits, Environmental research letters, 7, 044042, 2012.
678 Croci, E., Luechitta, B., and Molteni, T.: Low carbon urban strategies: An investigation of 124 European cities, Urban Climate,
679 40, 101022, <https://doi.org/10.1016/j.uclim.2021.101022>, 2021.
680 De Gennaro, M., Paffumi, E., and Martini, G.: Big Data for Supporting Low-Carbon Road Transport Policies in Europe: Applications, Challenges and Opportunities, Big Data Research, 6, 11-25, <https://doi.org/10.1016/j.bdr.2016.04.003>, 2016.
681 Field of Action: Transport: https://dibek.berlin.de/?lang=en#caption_c2c12, last access: 28/07/2025.
682 Dou, X., Hong, J., Ciais, P., Chevallier, F., Yan, F., Yu, Y., Huo, D., Sun, Y., Wang, Y., Davis, S. J., Crippa, M.,
683 Janssens-Maenhout, G., Guizzardi, D., Solazzo, E., Lin, X., Song, X., Zhu, B., Cui, D., Ke, P., Wang, H., Zhou, W., Huang,
684 X., Deng, Z., and Liu, Z.: Near-real-time global gridded daily CO2 emissions 2021, Scientific Data, 10, 69, 10.1038/s41597-023-01963-0, 2023.
685 EEA greenhouse gases — data viewer: <https://www.eea.europa.eu/en/analysis/maps-and-charts/greenhouse-gases-viewer-data-viewers?activeTab=570bee2d-1316-48cf-adde-4b64092119b>, last access: 28/07/2025.
686 Greenhouse gas emissions from transport in Europe: <https://www.eea.europa.eu/en/analysis/indicators/greenhouse-gas-emissions-from-transport?activeAccordion=309c5ef9-de09-4759-bc02-802370dfa366>, last access: 28/07/2025.
687 Gately, C. K., Hutyra, L. R., and Sue Wing, I.: Cities, traffic, and CO2: A multidecadal assessment of trends, drivers, and
688 scaling relationships, Proc Natl Acad Sci U S A, 112, 4999-5004, 10.1073/pnas.1421723112, 2015.
689 Guevara, M., Jorba, O., Tena, C., Denier van der Gon, H., Kuenen, J., Elguindi, N., Darras, S., Granier, C., and Pérez García-
690 Pando, C.: Copernicus Atmosphere Monitoring Service TEMPOral profiles (CAMS-TEMPO): global and European emission
691 temporal profile maps for atmospheric chemistry modelling, Earth Syst. Sci. Data, 13, 367-404, 10.5194/essd-13-367-2021,
692 2021.
693 Huo, D., Huang, X., Dou, X., Ciais, P., Li, Y., Deng, Z., Wang, Y., Cui, D., Benkhelifa, F., Sun, T., Zhu, B., Roest, G., Gurney,
694 K. R., Ke, P., Guo, R., Lu, C., Lin, X., Lovell, A., Appleby, K., DeCola, P. L., Davis, S. J., and Liu, Z.: Carbon Monitor Cities
695 near-real-time daily estimates of CO2 emissions from 1500 cities worldwide, Scientific Data, 9, 533, 10.1038/s41597-022-
696 01657-z, 2022.
697 Tomtom traffic index: <https://www.tomtom.com/traffic-index/about/>, last access: 28/07/2025.
698 Kennedy, C. A., Ibrahim, N., and Hoornweg, D.: Low-carbon infrastructure strategies for cities, Nature Climate Change, 4,
699 343-346, 10.1038/nclimate2160, 2014.
700 Transportation Sector - Global Road Emissions, Climate TRACE Emissions Inventory: <https://unfccc.int/climate-action/un-global-climate-action-awards/climate-leaders/city-of-paris>, last access: 28/07/2025.
701 Kühbacher, D., Aigner, P., Super, I., Droste, A., Denier van der Gon, H., Illic, M., and Chen, J.: Bottom-up estimation of traffic
702 emissions in Munich based on macroscopic traffic simulation and counting data, EGU General Assembly 2023, Vienna,
703 Austria, <https://doi.org/10.5194/egusphere-egu23-12997>, 2023.
704 Naiudomthum, S., Winijkul, E., and Sirisubtawee, S.: Near Real-Time Spatial and Temporal Distribution of Traffic Emissions
705 in Bangkok Using Google Maps Application Program Interface, 10.3390/atmos13111803, 2022.
706 Nakamura, K. and Hayashi, Y.: Strategies and instruments for low-carbon urban transport: An international review on trends
707 and effects, Transport Policy, 29, 264-274, <https://doi.org/10.1016/j.tranpol.2012.07.003>, 2013.
708 Ntziachristos, L., Gkatzoflias, D., Kouridis, C., and Samaras, Z.: COPERT: a European road transport emission inventory
709 model, Information Technologies in Environmental Engineering: Proceedings of the 4th International ICSC Symposium
710 Thessaloniki, Greece, May 28-29, 2009, 491-504,
711 Comptage routier - Données trafic issues des capteurs permanents: https://opendata.paris.fr/explore/dataset/comptages-routiers-permanents/information/?disjunctive.libelle&disjunctive.libelle_nd_amont&disjunctive.libelle_nd_aval&disjunctive.etat_trac, last access: 28/07/2025.
712 Ramírez, A., de Keizer, C., Van der Sluijs, J. P., Olivier, J., and Brandes, L.: Monte Carlo analysis of uncertainties in the
713 Netherlands greenhouse gas emission inventory for 1990–2004, Atmospheric Environment, 42, 8263-8272,
714 <https://doi.org/10.1016/j.atmosenv.2008.07.059>, 2008.

723 An introduction to explainable AI with Shapley values^①:
724 https://shap.readthedocs.io/en/latest/example_notebooks/overviews/An%20introduction%20to%20explainable%20AI%20with%20Shapley%20values.html, last access: 28/07/2025.
725
726 Shi, Q., Ciais, P., Megel, N., Bonnemaizon, X., Mittakola, R. T., Engelen, R., and Zhou, C.: High spatiotemporal resolution
727 traffic CO₂ emission maps derived from Floating Car Data (FCD) for 20 European cities (2023), Zenodo [dataset],
728 10.5281/zenodo.16600210, 2025.
729 Super, I., Dellaert, S. N. C., Visschedijk, A. J. H., and Denier van der Gon, H. A. C.: Uncertainty analysis of a European high-
730 resolution emission inventory of CO₂ and CO to support inverse modelling and network design, *Atmos. Chem. Phys.*, 20,
731 1795–1816, 10.5194/acp-20-1795-2020, 2020.
732 Ulrich, V., Brückner, J., Schultz, M., Vardag, S. N., Ludwig, C., Fürle, J., Zia, M., Lautenbach, S., and Zipf, A.: Private
733 Vehicles Greenhouse Gas Emission Estimation at Street Level for Berlin Based on Open Data, *ISPRS International Journal of
734 Geo-Information*, 12, 138, 2023.
735 USEPA: Motor Vehicle Emission Simulator: MOVES5, 2024.
736 Wen, Y., Wu, R., Zhou, Z., Zhang, S., Yang, S., Wallington, T. J., Shen, W., Tan, Q., Deng, Y., and Wu, Y.: A data-driven
737 method of traffic emissions mapping with land use random forest models, *Applied Energy*, 305,
738 10.1016/j.apenergy.2021.117916, 2022.
739 Xavier Bonnemaizon , P. C., Chuanlong Zhou, Simon Ben-Arous, Steven J Davis, Nicolas Megel: Scaling traffic variables
740 from sensors sample to the entire city at high spatiotemporal resolution with machine learning: applications to the Paris
741 megacity, <https://eartharxiv.org/repository/view/6948/>, 2024.
742 Zhao, Y., Nielsen, C. P., Lei, Y., McElroy, M. B., and Hao, J.: Quantifying the uncertainties of a bottom-up emission inventory
743 of anthropogenic atmospheric pollutants in China, *Atmos. Chem. Phys.*, 11, 2295–2308, 10.5194/acp-11-2295-2011, 2011.
744